Carbon 183 (2021) 1–11

Contents lists available at ScienceDirect

Carbon

journal homepage: www.elsevier.com/locate/carbon

Research Article

The importance of surface states in N-doped carbon quantum dots

Slavia Deeksha Dsouza [a, b, *], Marius Buerkle [a], Paul Brunet [b], Chiranjeevi Maddi [b], Dilli Babu Padmanaban [b], Alessio Morelli [b], Amir Farokh Payam [b], Paul Maguire [b], Davide Mariotti [b], Vladimir Svrcek [a]

[a] National Institute of Advanced Industrial Science and Technology (AIST) Central 2, Umezono 1-1-1, Tsukuba, Ibaraki, 305-8568, Japan
[b] Nanotechnology & Integrated Bio-Engineering Centre (NIBEC), Ulster University, Jordanstown, Newtownabbey, Co. Antrim, BT37 0QB, United Kingdom

ARTICLE INFO

Article history:
Received 28 January 2021
Received in revised form
19 May 2021
Accepted 30 June 2021
Available online 2 July 2021

Keywords:
Nitrogen doping
Quantum yield
Photoemission
Microplasma
Optical properties

ABSTRACT

Nitrogen-doped carbon quantum dots are synthesized by a one-step atmospheric pressure microplasma process. The origin of the observed photoluminescence emission and its relationship with nitrogen doping is studied using a range of optical and chemical measurements along with verification by theoretical calculations. Nitrogen doping into the core and functionalization of surface states with nitrogen and oxygen groups gives rise to a hybrid structure which is responsible for the luminescence with quantum yields up to 33%. Carrier multiplication is observed as a step-like enhancement in the quantum yield. The analysis of visible-light emission suggests that the emission originates for the most part from surface states and not due to recombination within the quantum dot core. The role of surface functional groups is dominant over quantum confinement in determining the optical properties.

1. Introduction

Photoluminescent nanomaterials have been widely explored in the past decade and many semiconductor nanocrystals, metal complexes, and carbon-based materials have given rise to a totally new field reporting fluorescent materials. The complex nature and a vast range of configurations of carbon-based materials have often complicated the understanding of related properties and their implementation in application devices. However, carbon-based materials are, in principle, to be favored to other semiconductor and metal complexes due to exceptional properties such as biocompatibility, ease of synthesis, low-cost, photo-stability, and low environmental impact [1]. However, for carbon to have a strong emission is a challenge because its bulk allotropes graphite and diamond are both non-luminescent due to the former being a conductor and the latter an insulator with indirect bandgap of 5.5 eV. Carbon nanostructures like single-/multi-walled carbon nanotubes and fullerenes exhibit interesting properties different from their bulk counterparts and efficient emission has been achieved, despite several challenges [2–4]. Carbon quantum dots (CQDs) have been widely explored by various research groups worldwide since they were first discovered by Xiaoyou Xu et al. in 2004 [5]. Carbon quantum dots are nanomaterials having sp^2 hybridized graphitic core with functionalized surface and size typically less than 10 nm. Several research groups have tried to explore the photoluminescence mechanism by studying the chemical structure and how the core structure and surface affect the energy states giving rise to radiative recombination [6–9].

CQDs with size-tunable optical properties and high quantum yields have been obtained by several top-down and bottom-up synthesis methods including hydrothermal or solvothermal [10–16], oxidative acid treatments [17,18], chemical-only methods [19], laser ablation [20], microwave treatments [21,22], electrochemical methods [3] etc. Using these methods, high quality CQDs have been obtained by appropriate choice of materials and reaction conditions [23,24]. However, obtaining controlled particle sizes often require post-synthesis treatment methods like washing, annealing, which are time and energy consuming. This could complicate manufacturing scalability and reproducibility. Instead of using thermal or chemical energy for the synthesis, energy from a plasma-liquid discharge can activate precursors and accelerate the formation of these CQDs and this allows the use of

* Corresponding author. Nanotechnology & Integrated Bio-Engineering Centre (NIBEC), Ulster University, Jordanstown, Newtownabbey, Co. Antrim, BT37 0QB, United Kingdom
E-mail addresses: Dsouza-SD@ulster.ac.uk (S.D. Dsouza), marius.buerkle@aist.go.jp (M. Buerkle).

https://doi.org/10.1016/j.carbon.2021.06.088

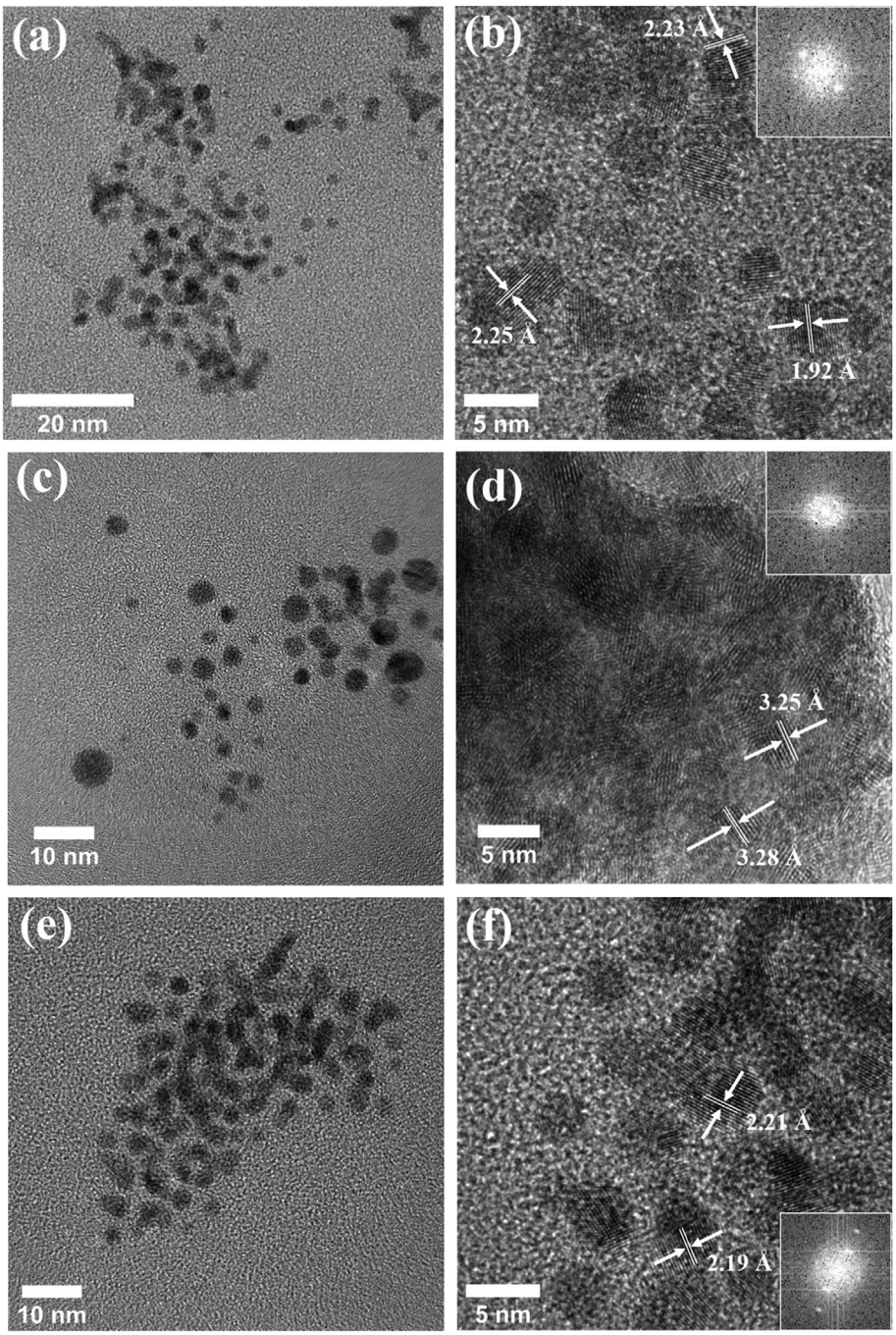

Fig. 1. TEM image and HR-TEM image with lattice spacing calculated by FFT (insets) of N-CQDs synthesized at 4 mA (a–b), 6 mA (c–d) and 8 mA (e–f).

temperature-sensitive or low-reactivity precursors [25]. These QDs can be functionalized and doped by electron-induced dissociation through so called plasma-induced non-equilibrium electrochemistry (PiNE) [26,27]. PiNE synthesis methods have been proven to result in CQDs in some cases with strong luminescence [28–31]. Using higher reaction temperatures as in thermal methods may result in the complete loss of surface functional groups which may reduce the luminescence and thus low-temperature and low-power synthesis methods should be preferred in some cases. For instance, the power needed to sustain a microplasma is low (12–24 W) compared to microwave methods (200–900 W) [30]. Surface functionalization by carboxyl, hydroxyl groups, and nitrogen doping of CQDs has proven to be effective in improving the optical properties and increasing in the quantum yield due to surface passivation [32,33].

We previously demonstrated the synthesis of nitrogen-doped CQDs (N-CQDs) by PiNE using an atmospheric pressure microplasma and have reported on the performance of solar cells with the N-CQDs used as an absorber layer [31]. Here we report on our investigations, involving both experiments as well as first-principles calculations, that reveal new insights in the origin of electronic transitions and that these are predominant at doped sites. We have been able to study the relationship between the structure, chemical composition, and emission properties of the N-CQDs thanks to our

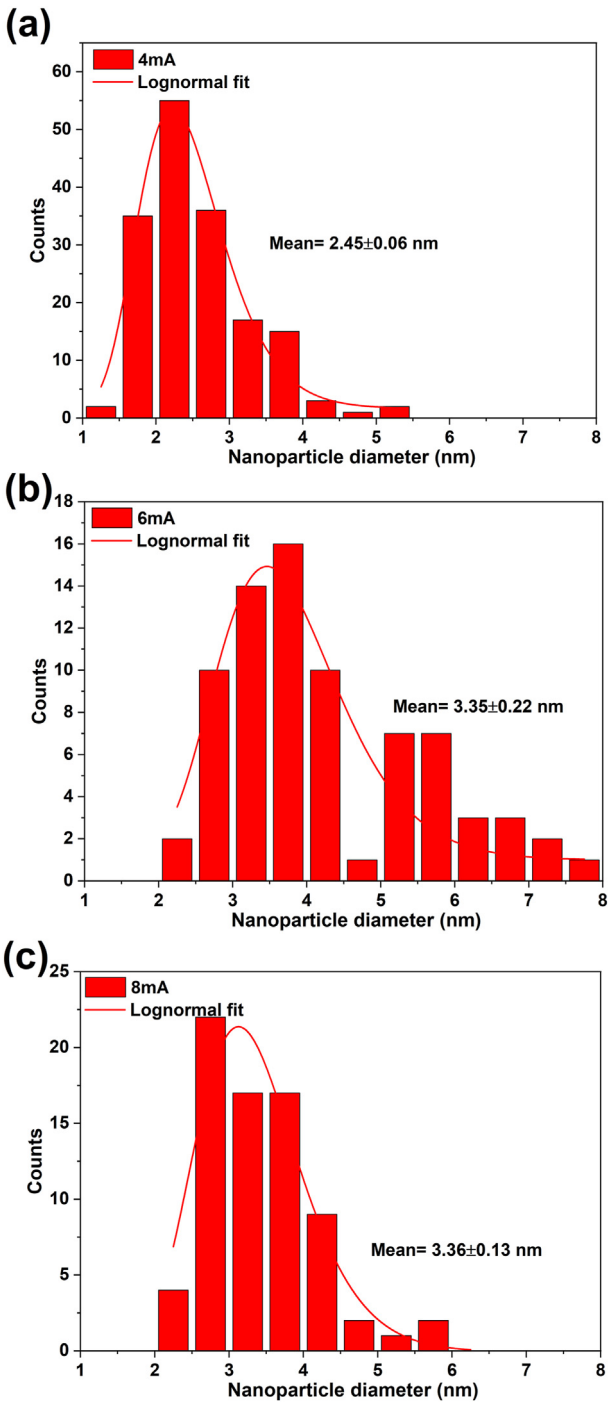

Fig. 2. Size distribution histograms with lognormal fit for N-CQDs synthesized at (a) 4 mA; (b) 6 mA and (c) 8 mA.

synthesis method, which allows for a reproducible approach to control substitutional vs. surface doping without impacting the QD morphology. We therefore discuss the changes in the photoluminescence emission, carrier multiplication, and how the absorption of N-CQDs leads to radiative recombination of excitons.

2. Experimental and theoretical calculation details

We synthesized N-CQDs following our PiNE method based on a microplasma [31] (Supporting Information, Fig. S1), using citric acid (CA) and ethylenediamine (EDA) as the carbon and nitrogen precursor, respectively. We prepared aqueous solutions with 1.051 g CA and 556 μL EDA. The microplasma was applied for 30 minutes as the cathode and a voltage of 3 kV was applied until the set current was reached. The set current was varied in the range 4–8 mA for different samples and the distance between the nickel tubing and the liquid surface was adjusted to be ~1.5 mm from the tip of capillary tube. The colour of the precursor solution changes during the course of the plasma process which indicates nanoparticle formation, and the colour change is more rapid for higher currents. All the measurements and characterization were carried out as soon as possible after synthesis unless otherwise stated.

Transmission electron microscopy (TEM) was carried out with a JEOL JEM-2100F microscope at an accelerating voltage of 200 kV. Colloidal samples were first drop-casted on ultra-thin carbon film on lacey carbon support films with 300 mesh gold or 200 mesh gold TEM grids (Agar Scientific) within a week from synthesis and dried at ambient conditions overnight; the analysis was carried out within the following week. Particle size analysis for the images with QDs that did not exhibit agglomeration, has been determined using ImageJ software. Images that showed a degree of agglomeration were analyzed and size estimated manually. Finally, some of the images that showed unclear boundaries between QDs were not considered in the size distribution determination. Atomic force microscopy (AFM) characterization was performed in air using a commercial system (D3100 Nanoscope III Digital Instruments, now Bruker) in amplitude modulation AFM (tapping mode). Topographic images were acquired at a scan rate of 1 Hz, with a silicon probe for soft tapping mode (FMV-A Bruker, spring constant 3 Nm^{-1}, resonance frequency 75 kHz, radius of curvature 10 nm). Samples for AFM were prepared by dip-coating 12 mm mica substrates in the as-prepared N-CQDs colloid within two weeks from synthesis and dried overnight; analysis was carried out within one day. This approach was developed after a few attempts with different methods and substrates. Mica substrates were utilized due to their low roughness which allowed identification of N-CQDs over the substrate. Using dip-coating and mica resulted in the possibility of finding isolated N-CQDs, which was not possible with the other methods. For X-ray photoelectron spectroscopy (XPS), N-CQDs were drop-casted on silicon substrates soon after synthesis and left to dry in ambient conditions overnight. Analysis was performed within one day from synthesis using an ESCALAB Xi^+ spectrometer microprobe (Thermo Fisher Scientific) with a focussed monochromatic Al Kα X-ray source ($h\nu = 1486.6$ eV, 650 μm spot size) operating at a power of 225 W (15 kV and 15 mA) and the photoelectrons were collected using a 180° double-focusing hemispherical analyser with a dual detector system. The energy scale of spectrometer was calibrated with sputter cleaned pure reference samples Au, Ag and Cu (Au $4f_{7/2}$, Ag $3d_{5/2}$ and Cu $3p_{3/2}$) positioned at binding energies 83.96, 368.21 and 932.62 eV, respectively. The base pressure in the analysis chamber was better than 5×10^{-9} mbar, which increased up to 5×10^{-7} mbar with charge neutraliser (flood gun) operated at 100 μA emission current. For the Fermi level alignment, a copper strip was used to make a good electrical contact between the sample and the spectrometer. Spectra were referenced against the Au core level and valence band spectra for charge compensation. For all the samples analyzed, the survey spectra were recorded with a step size of 1 eV and a pass energy of 150 eV and the narrow scans were recorded with a step size of 0.1 eV and a pass energy of 20 eV. This pass energy gives a 0.65 eV width for the Ag $3d_{5/2}$ peak measured on a sputter cleaned Ag sample. Data analysis and fitting were performed with Thermo Avantage software. After smart background subtraction, components in C 1s and N 1s core level spectra were adjusted using line shapes consisting of convolution products of a Gaussian (70%)

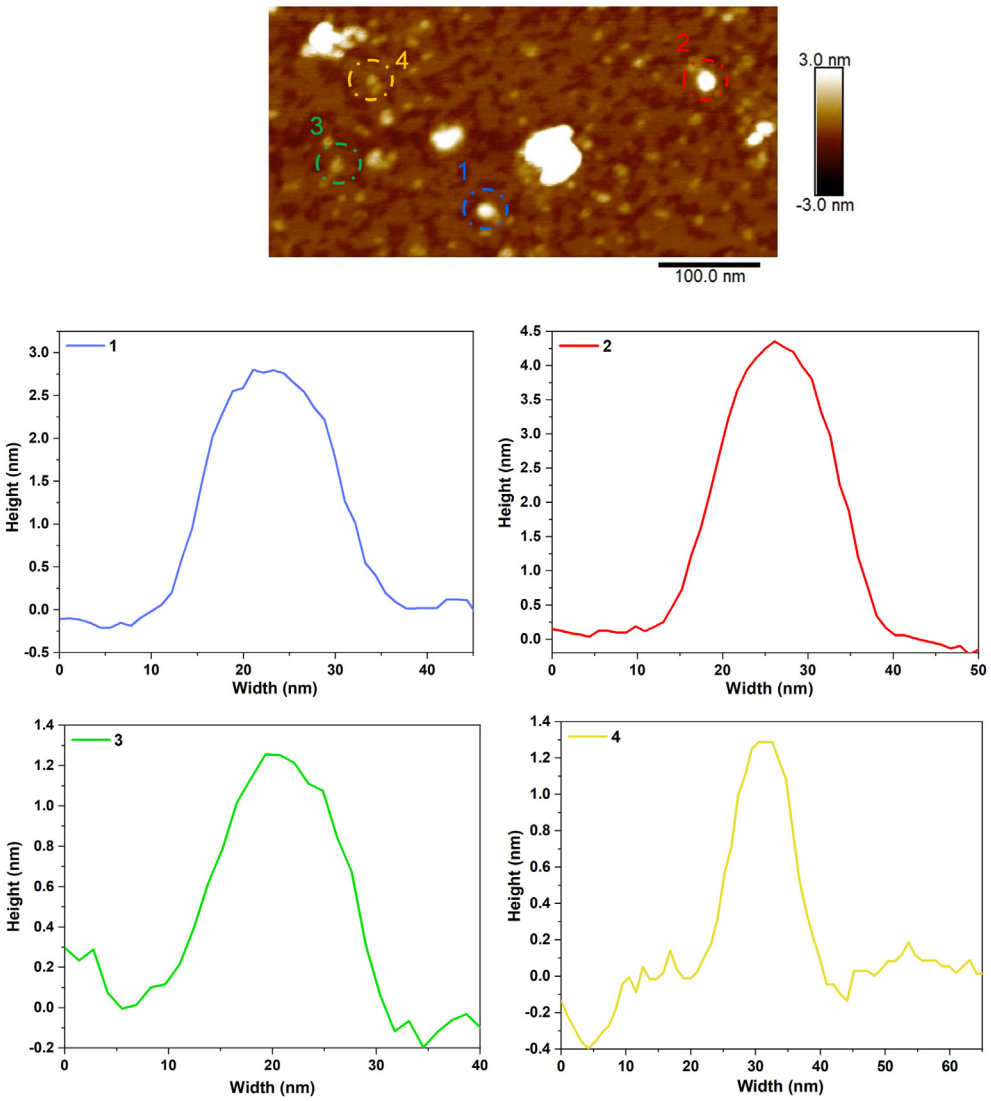

Fig. 3. AFM characterization of the N-CQDs at 6 mA on mica substrates: topography and line profiles of labelled N-CQDs. (colour).

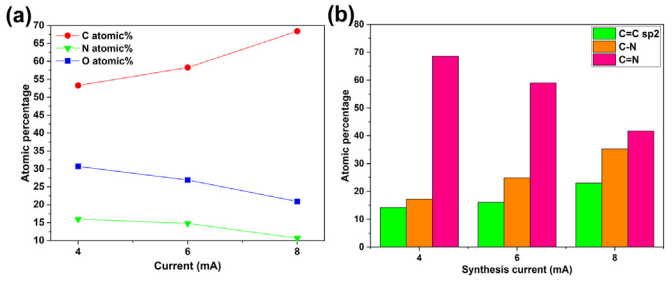

Fig. 4. (a) Variation of the carbon, oxygen and nitrogen atomic percentages as a function of the processing current from XPS survey spectra; (b) Atomic percentage variation of carbon components with processing current. (colour)

function and a Lorentzian (30%) function. Absorbance of the colloidal samples was measured soon after synthesis with a Perkin Elmer 1050 in transmission mode with deionized water as reference. Photoluminescence (PL) measurements were also taken from the colloidal samples soon after synthesis with an Agilent Technologies Cary Eclipse Fluorescence Spectrophotometer G9800A. For absolute quantum yield measurements, an integration sphere attached to a Horiba Jobin Yvon fluoromax-4 spectrometer was used to collect the PL of the N-CQDs. For excitation, a Xe lamp with a double monochromator was used, and the PL was detected by a charge coupled detector (CCD) mounted on a spectrograph via coupled ultraviolet-grade optical fiber. The excitation wavelength was selected through the monochromator. The emission spectra from N-CQDs film on quartz substrate and the reference from quartz were measured, and the number of emitted photons was then calculated from spectral integration. The number of absorbed photons was calculated using reduction of the excitation spectrum and comparing the sample and reference. The absolute QY is obtained as the ratio of the number of emitted photons to the number of absorbed photons. Measurements were performed in triplicates and the average value is reported for each excitation wavelength.

To elucidate the experimentally obtained optical properties we simulated the emission spectra of the CQDs using first-principles density functional theory (DFT) calculations at the level of linear response time dependent density functional theory (TD-DFT) within the Tamm-Dancoff approximation [34] as implemented in the quantum chemistry package *NWCHEM* [35]. We use the CAM-

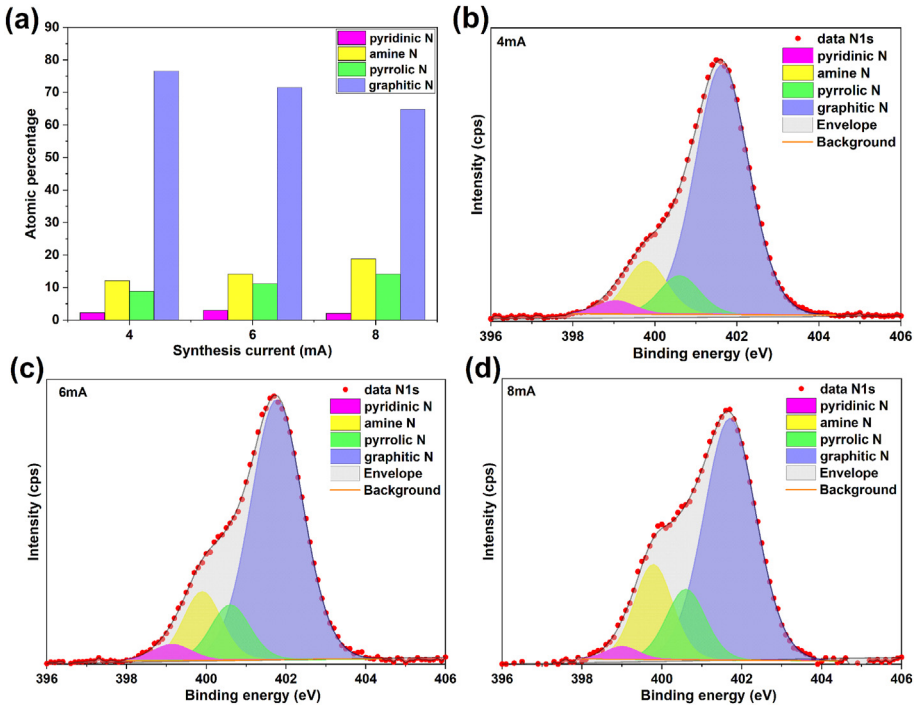

Fig. 5. (a) Atomic percentage variation of nitrogen components with processing current; High resolution XPS scan of the N 1s region for the samples processed at (b) 4 mA; (c) 6 mA and (d) 8 mA. (colour)

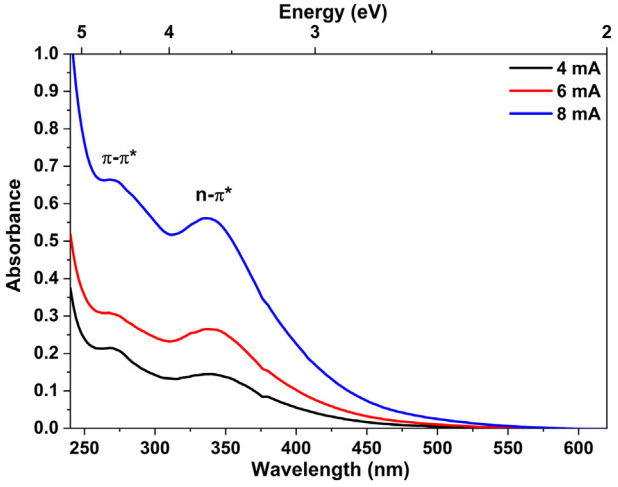

Fig. 6. Absorbance of the N-CQDs measured in colloid form. (colour)

QTP-02 functional [36] which tends to provide reliable excitation energies [37] and use the Los Alamos National Laboratory double-zeta basis set (LANL2DZdp) with diffuse and polarization functions [38] and the corresponding LANL2 ECP [39]. Total energies are converged with a precision of 10^{-7} a.u. and geometry optimization carried out until the maximum norm of the gradient drops below 10^{-4} a.u.

We model the CQD by 3 layers of approximately round graphene sheets with a diameter of ~1.4 nm passivated by hydrogen and with %2 of nitrogen doping to include both graphitic substitutional doping as well as pyrrolic nitrogen terminations. We first optimize within DFT the ground state geometry of the CQD model. Starting from the ground state geometry we optimize the CQD model for the lowest singlet excited state. Once we have obtained the optimized excited state geometry, we calculated for the $\boldsymbol{N}$ lowest lying excitation the excitation energies ε_i and corresponding oscillator strengths $\boldsymbol{\Omega_i}$ from which we can, assuming a Lorentzian broadening $\gamma = 0.2$ **eV**, obtain the optical spectra in the desired energy range as

$$\alpha(\boldsymbol{E}) \sim \sum_{\boldsymbol{i}}^{\boldsymbol{N}} \boldsymbol{\Omega_i} \frac{\lambda}{(\boldsymbol{E} - \varepsilon_{\boldsymbol{i}})^2 + \boldsymbol{\lambda}^2} \quad (1)$$

3. Results and discussion

TEM analysis shows that the N-CQDs are mostly spherical, generally well-dispersed. The TEM images of samples synthesized at different set discharge currents of 4 mA, 6 mA and 8 mA are given in Fig. 1a, 1c, and 1e and the corresponding size distributions in Fig. 2a–c, respectively. While we can provide a mean diameter based on lognormal fitting (2.45 nm, 3.35 nm, and 3.36 nm for N-CQDs synthesized at 4 mA, 6 mA, and 8 mA, respectively), we should note that the distributions present bimodal characters. We believe that this is due to the cylindrical shape (or *disc-*/*pancake*-like) of the quantum dots where the thickness is determined by the number of graphite layers (see more details further below). For this reason, the TEM size distributions result from the diameter distribution superimposed to the thickness (n. of graphite layers) distribution. This also contributes to an added degree of variability whereby the distribution also depends on the orientation of the N-CQDs on the TEM grid.

High resolution TEM (HR-TEM) images of the samples reveal the crystalline nature of the N-CQDs (Fig. 1b, d, 1f) and the lattice spacing was calculated by performing fast Fourier transform (FFT) (insets). We observed lattice spacing of 2.22–2.69 Å (~56% of the time), which we attribute to the (1120) lattice plane of graphene reported to be close to 2.42 Å [32,40–43]. We also observed values of 3.15–3.38 Å (~19% of the time) that can be attributed to the (002)

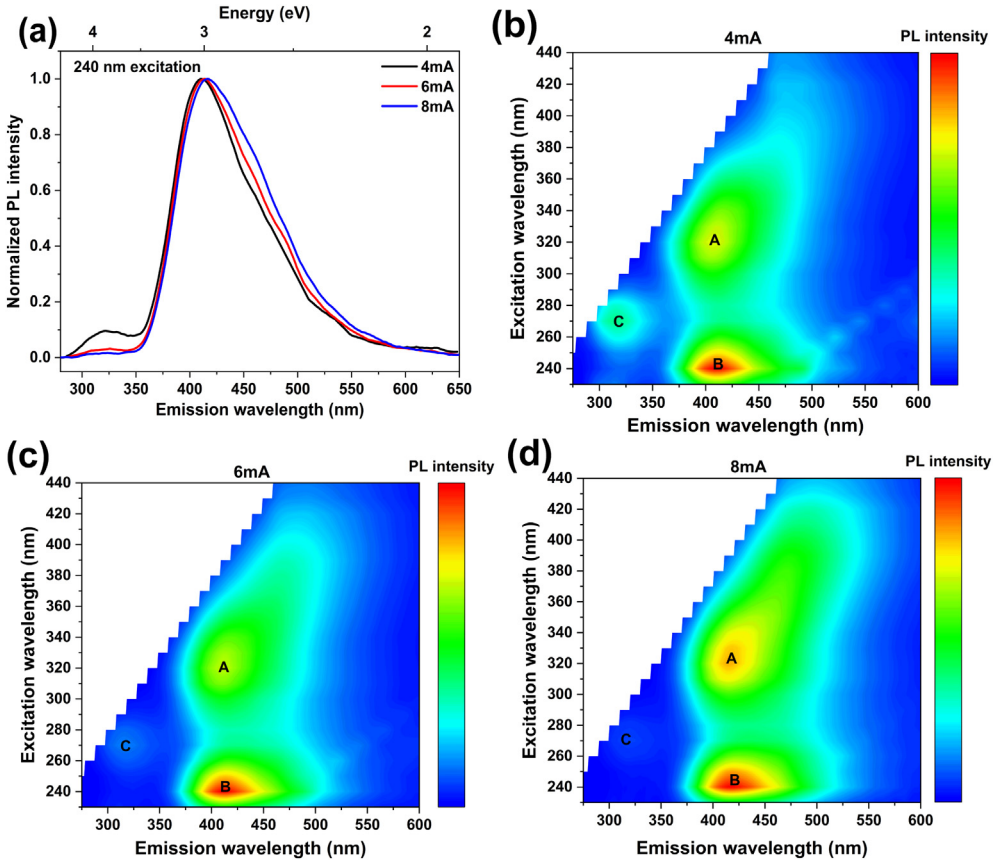

Fig. 7. (a) Normalized PL spectra of the maximum emission peak for each N-CQD sample in colloid form; 3-D colour mapped surface of excitation-emission spectra for the N-CQDs at (b) 4 mA; (c) 6 mA; (d) 8 mA (colour)

plane spacing reported for graphite (3.3 Å) [32,42] and values of 1.92–2.21 Å (~25% of the times) related to the (100) plane of graphite (2.0 Å) [44–46]. Although the lattice spacing is close to that of graphite, the values that we have observed have been also interpreted in the literature as due to nitrogen doping into the carbon core which may have induced disorder into the lattice [47–53]. These results also suggest that the N-CQDs exhibit a preferential orientation (56%) when on the grid, i.e. with the graphene plane parallel to the grid plane. The graphite spacing instead was observed more often when the samples showed some degree of agglomeration as seen in Fig. 1d, corroborating our observation about the bimodal character of the distributions. To understand better the 3-dimensional morphology of the N-CQD, AFM characterization was performed on the N-CQDs synthesized at 6 mA (Fig. 3). Due to the AFM tip convolution effect, the diameter of the N-CQDs measured with this technique is an overestimate and hence only the height of the discs-shaped N-CQDs is considered to be fully reliable [54]. The height measured from line profiles from the AFM images varied between 1.3 nm and 4.2 nm (Fig. 3) and thus from TEM and AFM results we can infer that these N-CQDs are formed by 4–12 layers of graphene and present a cylindrical shape.

Several reports in the literature suggest the dependency of the optical properties of N-CQDs on the chemical structure such as surface functionalization, the extent of nitrogen doping, and the position of nitrogen atoms (i.e. whether they are within the carbon core or on the surface) [9,55]. To study this, XPS was performed on the synthesized N-CQDs. The XPS survey spectra for all samples (Supporting Information, Fig. S2) show the presence of C, N, and O at binding energies around 285 eV, 400 eV and 531 eV, respectively. The atomic percentage of carbon, nitrogen, and oxygen with varying synthesis currents is given in Fig. 4a which shows increased carbon percentage and decreased nitrogen and oxygen relative content at higher current values. This could be due to preferential chemical pathways in the dissociation of the carbon precursor and may be responsible for the slightly larger particles at higher currents also resulting in a higher degree of doping at lower synthesis currents. We have then analyzed high resolution C 1s and N 1s spectra of the N-CQDs synthesized at 4–8 mA currents. Deconvolution of the spectra reveals the presence of C=C sp^2 at 284.6 eV [56–62], C–C/C–H at 285.2 eV [57,61,62], C–N at 285.8 eV [59,63–69], C–O at 286.5 eV [58,62,69–75], C=N at 287.2 eV [71,76], C=O at 288.3 eV [8,57,58,63,65,68–70,72,73,75,77–79], O–C=O at 289.0 eV [60,61,73–75], pyridinic nitrogen at 399.1 eV [45,58,71,80,81], amine groups at 399.9 eV [57,63,68], pyrrolic nitrogen at 400.6 eV [70,71,78,81,82] and graphitic nitrogen at 401.7 eV [8,32,57,58,68,70,78] (Fig. S3, Supporting Information and Fig. 5b–d for deconvoluted spectra). Generally, both the C and O peaks are easily affected by contamination where for instance adventitious carbon can present peaks corresponding to C–C/C–H, C–O and C=O. We have therefore focused on the peaks originating from C=C sp^2 bonds at 284.6 eV and carbon-nitrogen bonds at 285.8 eV (C–N) and 287.2 eV (C=N). We report in Fig. 4b (C 1s) and Fig. 5a (N 1s) the trends with processing current of atomic percentage of the atoms in the different chemical bond arrangements considered. The C=C sp^2 bond is characteristic of the CQDs. Of the carbon peaks involving bonds with nitrogen, C–N could originate from both the unreacted EDA precursor as well as from the N-CQDs, while the component corresponding to C=N is most likely to

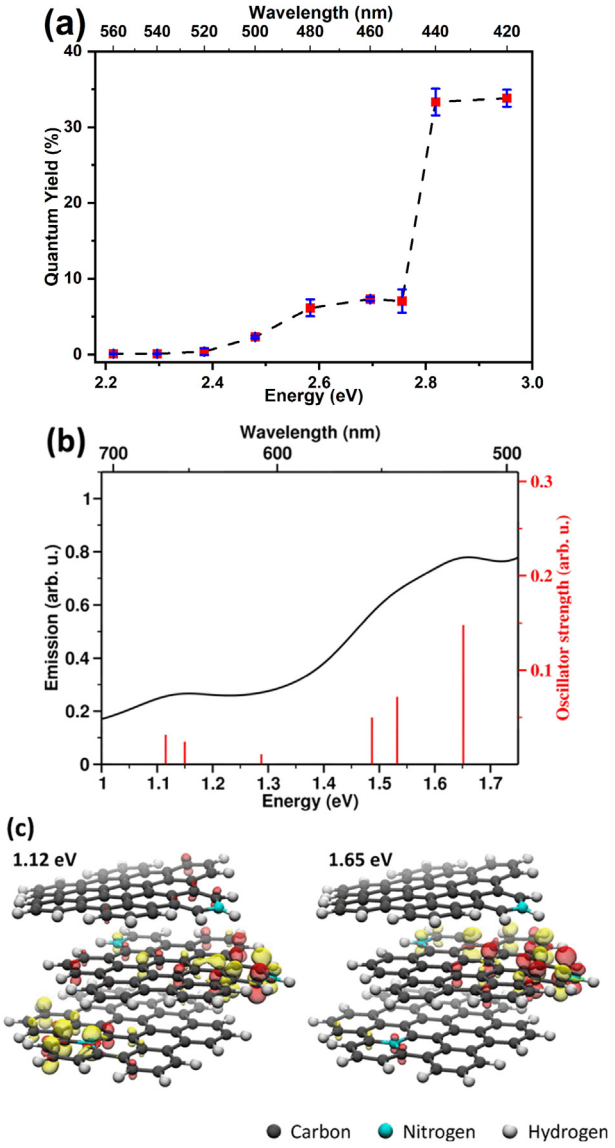

Fig. 8. (a) Excitation energy dependence of the absolute PL quantum yield at room temperature; (b) Calculated emission spectra, excitation energies and corresponding oscillator strength; onset of emission corresponds to 2 times the step up in the quantum yield as suggested in Ref. [93]; (c) Transition density for the excitation at 1.12 eV and 1.65 eV. The transition density is mainly localized around nitrogen atoms. Red isosurface corresponds to positive weight and yellow isosurface to negative respectively. (colour)

originate from pyridinic nitrogen doping of the QDs. The relative higher concentrations corresponding to C—N and C═N with respect to sp^2 bonds (Fig. 4b) suggest a very high degree of doping either at the core or at the surface of the N-CQDs. Also, while sp^2 bond contribution increases at higher current, C═N is decreasing which supports our previous suggestion inferred from Fig. 4a that CA decomposition is faster at higher currents; i.e. QD growth by carbon atoms is faster than nitrogen doping as the current is increased. The increasing trend of the C—N bond contribution further supports this idea and suggests surface doping by nitrogen increases with current increasing. The N 1s peak components (Fig. 5) on the other hand can be used to distinguish the type of nitrogen doping, where graphitic-N corresponds to doping within the core and pyrrolic-N and amine groups are mainly indicative of nitrogen bonds at the surface. Pyridinic-N can be present both within the core, therefore introducing defects, or at the surface. Fig. 5a shows that most of the nitrogen appears as graphitic, therefore indicating N-doping within the core for the most part. Graphitic-N decreases as the current is increased, corroborating a faster carbon precursor supply to the growth at higher current so that nitrogen atoms are incorporated less within the core of the N-CQDs and tend to bond at the surface instead, as the current is increased. This is further confirmed by the percentage corresponding to pyrrolic-N and amine groups, which can be associated with surface terminations, and that increase with increasing current. As pyridinic-N can represent nitrogen both at the surface as well as within the core, the trend is representative of a mixed behavior. Hydrogen and oxygen-based surface states are also likely to be present as shown by the C—C/C—H peak at 285.2 eV, C—O at 286.5 eV, C═O at 288.3 eV and O-C═O at 289.0 eV (Supporting Information, Fig. S3). Overall, the XPS analysis shows that in addition to hydrogen and limited oxygen-based terminations, which are expected based on the formation mechanisms reported in the literature (see further below), N-CQDs are terminated by N-groups and with substitutional nitrogen (graphitic) doping being predominant. A higher processing current seems to limit N-doping and accelerate QDs growth with a faster carbonization. CA and EDA are in competition when contributing to the growth of the QDs. As the carbon supply from CA prevails, N-doping at the core is reduced and will tend instead to bond at the surface. This is also supported by the decrease in I_D/I_G ratio at higher current as shown by the Raman spectra (Supporting Information, Fig. S4).

There have been a number of reports in literature on the growth mechanisms of CQDs and N-CQDs [32,56,83–85]. These suggest that the precursors CA and EDA self-assemble to form a large network with formation of amide bonds due to intermolecular and intramolecular dehydration and polymerization among the carboxylic, hydroxyl and amine groups. This results in a carbon core structures with N-atoms incorporated as pyridinic, pyrrolic, amide, and graphitic entities leading to N-CQD formation [32,56,84,85]. The synthesis of N-CQDs by PiNE follows very similar growth mechanisms, where plasma-induced reactions accelerate the delivery of precursors but also localize CQD formation in a small volume below the plasma-liquid interface. The localization is important as it provides a different degree of control on the growth that does not depend on precursor concentrations. Compared to other microplasma-based synthesis of carbon dots, our method is proven beneficial due to reduced reaction time, crystalline structure of the N-CQDs, and higher QY [29,30].

The absorbance of the N-CQDs in colloid form (diluted 50 mg in 10 mL water) is measured in a 10 mm quartz cuvette with deionized water as reference and the resulting spectra for varying discharge currents are given in Fig. 6. All samples show similar patterns with the onset of absorption in the visible region, higher absorbance in the ultraviolet (UV) region and a couple of peaks. The absorbance in the UV region around 270 nm can be attributed to $\pi \rightarrow \pi^*$ transitions where the π states are the aromatic sp^2 hybridized carbon atoms in the core.

The absorbance peak at around 340 nm can be assigned to $n \rightarrow \pi^*$ transitions which could indicate absorption by nitrogen or oxygen containing groups at the surface of the N-CQDs [55,86]. With increase in discharge current, the absorbance seems to maintain the same spectra however with an overall increase in intensity. This indicates that a larger number of N-CQDs are produced, consistent with the ability of the process to decompose CA at a faster rate when the current is higher. A closer analysis also shows that the absorbance intensity corresponding to the $n \rightarrow \pi^*$ transitions is higher with respect to that of the $\pi \rightarrow \pi^*$ transitions for higher processing current, therefore the absorbing surface states have increased for the N-CQDs synthesized at 6 mA and 8 mA

(corresponding intensity ratios are 0.66, 0.83 and 0.83). This is in very good agreement with the XPS analysis. The Tauc plots are given in Figs. S6a–c (Supporting Information), which yield direct bandgap values of 3.17 eV, 3.17 eV and 3.15 eV for 4 mA, 6 mA and 8 mA samples. If an indirect bandgap is considered (Figs. S7a–c), the values are 2.46 eV, 2.44 eV and 2.38 eV for 4 mA, 6 mA and 8 mA samples respectively. Both direct and indirect bandgap values are smaller for higher processing current. Graphitic nitrogen and surface nitrogen atoms have presence of lone pair of electrons which results in positive charge due to electron donation to the carbon structure thus increasing the electron density which reduces the bandgap [9,87]. In this way the electronic structure of the N-CQDs and the absorption tails depend on the charge transfer and also frontier orbital hybridization between the carbon core and surface functional groups [88,89]. A slight decrease of the bandgap is therefore consistent with a decrease in substitutional doping at higher current as observed in our XPS analysis (Fig. 5a).

The photoluminescence (PL) measurements (240 nm excitation) for the N-CQDs synthesized with varying processing currents result in maximum emission intensities at wavelength 410 nm, 414 nm, 417 nm for 4 mA, 6 mA and 8 mA samples as shown in the normalized PL spectra in Fig. 7a. The data has been normalized to the emission maxima. The small red-shift of the emission wavelength could be linked to the small reduction in the bandgap for the N-CQD synthesized at higher current, however this is superimposed onto surface-state emission (see below) [67]. Colored-coded maps of the photoemission are given in Fig. 7b–d with emission wavelength in the x-axis, excitation in y-axis and the colour scale giving the PL intensity, (the full set of PL emission spectra for each excitation can be found in the Supporting Information, Figs. S9 and S10). For all the samples, the excitation-emission figures show similar patterns with three different regions excited at different wavelengths, labelled as “A”, “B” and “C”. Bandgap emission is expected to be affected by size distribution for each sample and therefore would appear as an elongated pattern in Fig. 7 [87]. This corresponds for instance to the emission that peaks in the range 400–450 nm and excited by ~320 nm (A). This is also sufficiently close to the indirect bandgap (2.38–2.46 eV) for all samples and we can therefore attribute it to bandgap emission from the core of the N-CQDs and originating from above-bandgap energy levels. This core bandgap emission is however relatively weak, and we can observe that lower excitation wavelengths offer different emission pathways. The strongest emission for all samples is for instance in the same region (400–450 nm) but excited at ~240 nm (B). This appears to be different than emission from the core bandgap transitions and it is specifically excited only with a narrow range of wavelengths; it therefore appears as a confined and non-elongated spot (B) in Fig. 7. This emission originates from UV absorption and excitons may have sufficient energy to recombine in different states from where they have been produced. It is therefore likely that this emission is associated with surface states which may include transitions due to N, associated with pyrrolic and amine groups, or O surface states, edge states and molecular states [90]. Finally, Fig. 7b, corresponding to the sample produced at 4 mA, also shows a noticeable emission at 300–325 nm, excited with ~270 nm (C); this is progressively weaker for increasing current in Fig. 7b–c. The emission originates from EDA precursor (see Supporting Information) and suggests that this is consumed more effectively at higher current, possibly due to increasing surface doping over a greater total surface area. This is again in agreement with our previous absorbance results that indicated a higher number of N-CQDs synthesized with increasing current. Overall Fig. 7 shows that emission is dominated by surface states (B) with weak emission from bandgap transitions (A). This is also in agreement with previous reports [91,92]. Therefore, to manipulate the emission of CQDs, varying the nature and density of surface functional groups is the most direct way to produce considerable modification of PL whereas quantum confinement effect or core doping in CQDs is far less effective. This is also confirmed by Deng et al. while studying the optical properties of separated fragments of carbon dots with high colloidal stability by gradient-based centrifugation method [69]. We have observed that the emission properties of these N-CQDs in colloidal form are stable over time and also under given operational conditions (e.g. under prolonged illumination, see section G in the Supporting Information); however, the impact of film formation steps from the colloid, including annealing has shown some changes in the emission patterns (section F of the Supporting Information) that will need to be investigated fully in order to effectively integrate N-CQDs in application devices.

The absolute quantum yield (QY) was determined using an integrating sphere attached to the photoluminescence spectrometer. The QY varied up to 33% for the 6 mA sample. Interestingly, the QY also depends on the excitation energy (Fig. 8a). At low excitation energy (between 2.2 eV and 2.4 eV), the QY was measured to be below 0.2% which increased in a step like fashion to around 7% (from 2.5 to 2.7 eV) and finally rapidly reaches 33% as the selected excitation energy was increased to around 2.8 - 3 eV.

As demonstrated in Ref. [93] such step-like enhancement of the QY could point to carrier multiplication occurring in these CQDs [94]. Steps in the QY occur at integer multiples of the excitation energies in the emission spectra, essentially a single absorbed photon of energy E_0 leads to the emission of N photons with energy E_0/N. As we cannot experimentally observe the emission spectra excited with energies below 2 eV, it is not possible to directly probe the multiphoton emission correlated with the observed step-like behavior of the QY. Therefore, we calculated the emission spectra of CQDs with a diameter of around 1.4 nm and with 2% nitrogen doping using TD-DFT. While the CQD considered in the simulations are at the lower end of the size distribution, they should be sufficiently large, as we did only observe a weak size dependence of the optical properties in experiment and, as we see in the following, the emission properties are correlated with localized electronic transition. Fig. 8b shows the emission spectra for the relevant energy range; we can see that QY step (at ~2.8 eV, Fig. 8a) corresponds to twice the onset energy in the calculated spectrum (at ~1.4 eV, Fig. 8b). The corresponding transition densities [95] of the corresponding excitations (Fig. 8c and Fig. S13 in Supporting Information) show that the relevant electronic excitations occur localized at the vicinity of the nitrogen dopants. Furthermore, at higher energy the emission appears to be more concentrated at the surface terminations and although the excitation energy is not comparable, it is in qualitative agreement with our PL results.

4. Conclusions

Crystalline N-CQDs are obtained using a one-step, environmentally friendly and easy synthesis process. We have studied the optical properties combined with an in-depth chemical, structural, and morphological characterization. Prominent emission bands show emission from both core transitions and surface groups, where the latter is by far dominant. The change in synthesis conditions, precisely increasing the current, allows for a reduction of substitutional nitrogen doping in favor of surface states that are more efficient in their emission. In this way, we open the possibility of direct tunability control over doping, that within the range studied has no impact on other properties. The observation of emission originating from carrier multiplication is confirmed with first-principles calculations, however this remains limited and secondary to the emission originating from surface states. This

work has therefore shown avenues to control the degree of doping at the surface vs. substitutional doping, with the first far more efficient for enhancing emission properties. These results also suggest that this synthesis technique offers methodologies for synthesizing doped CQDs with a variety of precursors, including those that are temperature-sensitive and that these may allow to tailor emission to desired requirements for optoelectronic applications.

CRediT authorship contribution statement

Slavia Deeksha Dsouza: Investigation, Formal analysis, Data curation, Writing – original draft. **Marius Buerkle:** Investigation, Software, Formal analysis, Writing – original draft. **Paul Brunet:** Investigation. **Chiranjeevi Maddi:** Investigation, Formal analysis, Writing – original draft. **Dilli Babu Padmanaban:** Validation. **Alessio Morelli:** Investigation, Formal analysis, Writing – original draft. **Amir Farokh Payam:** Investigation, Formal analysis, Writing – original draft. **Paul Maguire:** Conceptualization, Methodology, Visualization, Supervision, Resources, Funding acquisition, Writing – review & editing. **Davide Mariotti:** Conceptualization, Methodology, Visualization, Supervision, Resources, Funding acquisition, Writing – review & editing. **Vladimir Svrcek:** Conceptualization, Methodology, Visualization, Supervision, Resources, Funding acquisition, Writing – review & editing.

Declaration of competing interest

The authors declare that they have no known competing financial interests or personal relationships that could have appeared to influence the work reported in this paper.

Acknowledgements

The authors thank Ulster University, National Institute of Advanced Industrial Science and Technology (AIST) and Engineering and Physical Sciences Research Council (EPSRC) (EP/M024938/1, EP/K022237/1, EP/R008841/1) for the financial support. S.D.D acknowledges the financial support from Department for Economy NI (PhD Studentship and USI-146). M.B. and V.S acknowledge the support by Kakenhi (20H02579) by the Japanese Society for the Promotion of Science. A.M. acknowledges funding from Invest Northern Ireland (RD0713920) and the European Union's INTERREG VA Programme, managed by the Special EU Programmes Body (SEUPB). We would like to acknowledge the contribution of Dr Darragh Carolan who has carried out initial experiments that motivated the work reported in this publication.

Appendix A. Supplementary data

Supplementary data to this article can be found online at https://doi.org/10.1016/j.carbon.2021.06.088.

References

[1] H. Liu, Z. Li, Y. Sun, X. Geng, Y. Hu, H. Meng, J. Ge, L. Qu, Synthesis of luminescent carbon dots with ultrahigh quantum yield and inherent folate receptor-positive cancer cell targetability, Sci. Rep. 8 (2018) 1–8, https://doi.org/10.1038/s41598-018-19373-3.
[2] Y. Lin, B. Zhou, R.B. Martin, K.B. Henbest, B.A. Harruff, J.E. Riggs, Z.X. Guo, L.F. Allard, Y.P. Sun, Visible luminescence of carbon nanotubes and dependence on functionalization, J. Phys. Chem. Lett. B. 109 (2005) 14779–14782, https://doi.org/10.1021/jp053073j.
[3] J. Zhou, C. Booker, R. Li, X. Zhou, T.K. Sham, X. Sun, Z. Ding, An electrochemical avenue to blue luminescent nanocrystals from multiwalled carbon nanotubes (MWCNTs), J. Am. Chem. Soc. 129 (2007) 744–745, https://doi.org/10.1021/ja0669070.
[4] S. Iijima, Helical microtubules of graphitic carbon, Nature 354 (1991) 56–58, https://doi.org/10.1038/354056a0.
[5] X. Xu, R. Ray, Y. Gu, H.J. Ploehn, L. Gearheart, K. Raker, W.A. Scrivens, Electrophoretic analysis and purification of fluorescent single-walled carbon nanotube fragments, J. Am. Chem. Soc. 126 (2004) 12736–12737, https://doi.org/10.1021/ja040082h.
[6] J. Du, H. Wang, L. Wang, S. Zhu, Y. Song, B. Yang, H. Sun, Insight into the effect of functional groups on visible-fluorescence emissions of graphene quantum dots, J. Mater. Chem. C. 4 (2016) 2235–2242, https://doi.org/10.1039/c6tc00548a.
[7] Q. Fang, Y. Dong, Y. Chen, C.H. Lu, Y. Chi, H.H. Yang, T. Yu, Luminescence origin of carbon based dots obtained from citric acid and amino group-containing molecules, Carbon N. Y. 118 (2017) 319–326, https://doi.org/10.1016/j.carbon.2017.03.061.
[8] K. Holá, M. Sudolská, S. Kalytchuk, D. Nachtigallová, A.L. Rogach, M. Otyepka, R. Zboril, Graphitic nitrogen triggers red fluorescence in carbon dots, ACS Nano 11 (2017) 12402–12410, https://doi.org/10.1021/acsnano.7b06399.
[9] S.H. Jin, D.H. Kim, G.H. Jun, S.H. Hong, S. Jeon, Tuning the photoluminescence of graphene quantum dots through the charge transfer effect of functional groups, ACS Nano 7 (2013) 1239–1245, https://doi.org/10.1021/nn304675g.
[10] S. Yang, J. Sun, X. Li, W. Zhou, Z. Wang, P. He, G. Ding, X. Xie, Z. Kang, M. Jiang, Large-scale fabrication of heavy doped carbon quantum dots with tunable-photoluminescence and sensitive fluorescence detection, J. Mater. Chem. A. 2 (2014) 8660–8667, https://doi.org/10.1039/c4ta00860j.
[11] G. Wang, Q. Guo, D. Chen, Z. Liu, X. Zheng, A. Xu, S. Yang, G. Ding, Facile and highly effective synthesis of controllable lattice sulfur-doped graphene quantum dots via hydrothermal treatment of durian, ACS Appl. Mater. Interfaces 10 (2018) 5750–5759, https://doi.org/10.1021/acsami.7b16002.
[12] A.B. Bourlinos, A. Stassinopoulos, D. Anglos, R. Zboril, V. Georgakilas, E.P. Giannelis, Photoluminescent carbogenic dots, Chem. Mater. 20 (2008) 4539–4541, https://doi.org/10.1021/cm800506r.
[13] B. Yin, J. Deng, X. Peng, Q. Long, J. Zhao, Q. Lu, Q. Chen, H. Li, H. Tang, Y. Zhang, S. Yao, Green synthesis of carbon dots with down- and up-conversion fluorescent properties for sensitive detection of hypochlorite with a dual-readout assay, Analyst 138 (2013) 6551–6557, https://doi.org/10.1039/c3an01003a.
[14] B.R. Selvi, D. Jagadeesan, B.S. Suma, G. Nagashankar, M. Arif, K. Balasubramanyam, M. Eswaramoorthy, T.K. Kundu, Intrinsically fluorescent carbon nanospheres as a nuclear targeting vector: delivery of membrane-impermeable molecule to modulate gene expression in vivo, Nano Lett. 8 (2008) 3182–3188, https://doi.org/10.1021/nl801503m.
[15] R. Liu, D. Wu, S. Liu, K. Koynov, W. Knoll, Q. Li, An aqueous route to multicolor photoluminescent carbon dots using silica spheres as carriers, Angew. Chem. Int. Ed. 48 (2009) 4598–4601, https://doi.org/10.1002/anie.200900652.
[16] S. Yang, X. Wang, P. He, A. Xu, G. Wang, J. Duan, Y. Shi, G. Ding, Graphene quantum dots with pyrrole N and pyridine N: superior reactive oxygen species generation efficiency for metal-free sonodynamic tumor therapy, Small 17 (2021) 2004867, https://doi.org/10.1002/smll.202004867.
[17] S.C. Ray, A. Saha, N.R. Jana, R. Sarkar, Fluorescent carbon nanoparticles: synthesis, characterization, and bioimaging application, J. Phys. Chem. C 113 (2009) 18546–18551, https://doi.org/10.1021/jp905912n.
[18] H. Liu, T. Ye, C. Mao, Fluorescent carbon nanoparticles derived from candle soot, Angew. Chem. Int. Ed. 46 (2007) 6473–6475, https://doi.org/10.1002/anie.200701271.
[19] Y. Li, X. Zhong, A.E. Rider, S.A. Furman, K. Ostrikov, Fast, energy-efficient synthesis of luminescent carbon quantum dots, Green Chem. 16 (2014) 2566–2570, https://doi.org/10.1039/c3gc42562b.
[20] Y.-P. Sun, B. Zhou, Y. Lin, W. Wang, K.A.S. Fernando, P. Pathak, M.J. Meziani, B.A. Harruff, X. Wang, H. Wang, P.G. Luo, H. Yang, M.E. Kose, B. Chen, L.M. Veca, S.-Y. Xie, Quantum-sized carbon dots for bright and colorful photoluminescence, J. Am. Chem. Soc. 128 (2006) 7756–7757, https://doi.org/10.1021/ja062677d.
[21] H. Zhu, X. Wang, Y. Li, Z. Wang, F. Yang, X. Yang, Microwave synthesis of fluorescent carbon nanoparticles with electrochemiluminescence properties, Chem. Commun. (2009) 5118–5120, https://doi.org/10.1039/b907612c.
[22] T.N.J.I. Edison, R. Atchudan, M.G. Sethuraman, J.J. Shim, Y.R. Lee, Microwave assisted green synthesis of fluorescent N-doped carbon dots: cytotoxicity and bio-imaging applications, J. Photochem. Photobiol. B Biol. 161 (2016) 154–161, https://doi.org/10.1016/j.jphotobiol.2016.05.017.
[23] Z. Kang, S.T. Lee, Carbon dots: advances in nanocarbon applications, Nanoscale 11 (2019) 19214–19224, https://doi.org/10.1039/c9nr05647e.
[24] C. Zhu, S. Yang, G. Wang, R. Mo, P. He, J. Sun, Z. Di, Z. Kang, N. Yuan, J. Ding, G. Ding, X. Xie, A new mild, clean and highly efficient method for the preparation of graphene quantum dots without by-products, J. Mater. Chem. B. 3 (2015) 6871–6876, https://doi.org/10.1039/c5tb01093d.
[25] L. Lin, Q. Wang, Microplasma: a new generation of Technology for functional nanomaterial synthesis, Plasma Chem. Plasma Process. 35 (2015) 925–962, https://doi.org/10.1007/s11090-015-9640-y.
[26] R. McGlynn, S. Chakrabarti, B. Alessi, H.S. Moghaieb, P. Maguire, H. Singh, D. Mariotti, Plasma-induced non-equilibrium electrochemistry synthesis of nanoparticles for solar thermal energy harvesting, Sol. Energy 203 (2020) 37–45, https://doi.org/10.1016/j.solener.2020.04.004.
[27] D. Sun, C. Maddi, C. Rafferty, M. Tang, M. Chen, B.G. Falzon, G. Sarri, D. Mariotti, P. Maguire, D. Sun, Effect of precursor pH on AuNP/MWCNT nanocomposites synthesized by plasma-induced non-equilibrium electrochemistry, J. Phys. D Appl. Phys. 53 (2020) 425207, https://doi.org/10.1088/1361-6463/ab9ee7.

[28] X. Huang, Y. Li, X. Zhong, A.E. Rider, K. Ostrikov, Fast microplasma synthesis of blue luminescent carbon quantum dots at ambient conditions, Plasma Process. Polym. 12 (2015) 59–65, https://doi.org/10.1002/ppap.201400133.
[29] X. Ma, S. Li, V. Hessel, L. Lin, S. Meskers, F. Gallucci, Synthesis of luminescent carbon quantum dots by microplasma process, Chem. Eng. Process. Process Intensif. 140 (2019) 29–35, https://doi.org/10.1016/j.cep.2019.04.017.
[30] X. Ma, S. Li, V. Hessel, L. Lin, S. Meskers, F. Gallucci, Synthesis of N-doped carbon dots via a microplasma process, Chem. Eng. Sci. 220 (2020) 115648, https://doi.org/10.1016/j.ces.2020.115648.
[31] D. Carolan, C. Rocks, D.B. Padmanaban, P. Maguire, V. Svrcek, D. Mariotti, Environmentally friendly nitrogen-doped carbon quantum dots for next generation solar cells, Sustain. Energy Fuels 1 (2017) 1611–1619, https://doi.org/10.1039/c7se00158d.
[32] D. Qu, M. Zheng, L. Zhang, H. Zhao, Z. Xie, X. Jing, R.E. Haddad, H. Fan, Z. Sun, Formation mechanism and optimization of highly luminescent N-doped graphene quantum dots, 5294, Sci. Rep. 4 (2014), https://doi.org/10.1038/srep05294, 1–11.
[33] Y. Dong, H. Pang, H. Bin Yang, C. Guo, J. Shao, Y. Chi, C.M. Li, T. Yu, Carbon-based dots Co-doped with nitrogen and sulfur for high quantum yield and excitation-independent emission, Angew. Chem. Int. Ed. 52 (2013) 7800–7804, https://doi.org/10.1002/anie.201301114.
[34] S. Hirata, M. Head-Gordon, Time-dependent density functional theory within the Tamm-Dancoff approximation, Chem. Phys. Lett. 314 (1999) 291–299, https://doi.org/10.1016/S0009-2614(99)01149-5.
[35] M. Valiev, E.J. Bylaska, N. Govind, K. Kowalski, T.P. Straatsma, H.J.J. Van Dam, D. Wang, J. Nieplocha, E. Apra, T.L. Windus, W.A. de Jong, NWChem: a comprehensive and scalable open-source solution for large scale molecular simulations, Comput. Phys. Commun. 181 (2010) 1477–1489, https://doi.org/10.1016/j.cpc.2010.04.018.
[36] R.L.A. Haiduke, R.J. Bartlett, Non-empirical exchange-correlation parameterizations based on exact conditions from correlated orbital theory, J. Chem. Phys. 148 (2018) 184106, https://doi.org/10.1063/1.5025723.
[37] R.L.A. Haiduke, R.J. Bartlett, Communication: can excitation energies be obtained from orbital energies in a correlated orbital theory, J. Chem. Phys. 149 (2018) 131101, https://doi.org/10.1063/1.5052442.
[38] C.E. Check, T.O. Faust, J.M. Bailey, B.J. Wright, T.M. Gilbert, L.S. Sunderlin, Addition of polarization and diffuse functions to the LANL2DZ basis set for P-block elements, J. Phys. Chem. 105 (2001) 8111–8116, https://doi.org/10.1021/jp011945l.
[39] W.R. Wadt, P.J. Hay, Ab initio effective core potentials for molecular calculations. Potentials for main group elements Na to Bi, J. Chem. Phys. 82 (1985) 284–298, https://doi.org/10.1063/1.448800.
[40] J. Peng, W. Gao, B.K. Gupta, Z. Liu, R. Romero-Aburto, L. Ge, L. Song, L.B. Alemany, X. Zhan, G. Gao, S.A. Vithayathil, B.A. Kaipparettu, A.A. Marti, T. Hayashi, J.J. Zhu, P.M. Ajayan, Graphene quantum dots derived from carbon fibers, Nano Lett. 12 (2012) 844–849, https://doi.org/10.1021/nl2038979.
[41] S. Yang, J. Sun, P. He, X. Deng, Z. Wang, C. Hu, G. Ding, X. Xie, Selenium doped graphene quantum dots as an ultrasensitive redox fluorescent switch, Chem. Mater. 27 (2015) 2004–2011, https://doi.org/10.1021/acs.chemmater.5b00112.
[42] D. Qu, M. Zheng, P. Du, Y. Zhou, L. Zhang, D. Li, H. Tan, Z. Zhao, Z. Xie, Z. Sun, Highly luminescent S, N co-doped graphene quantum dots with broad visible absorption bands for visible light photocatalysts, Nanoscale 5 (2013) 12272–12277, https://doi.org/10.1039/c3nr04402e.
[43] J. Li, S. Yang, Z. Liu, G. Wang, P. He, W. Wei, M. Yang, Y. Deng, P. Gu, X. Xie, Z. Kang, G. Ding, H. Zhou, X. Fan, Imaging cellular aerobic glycolysis using carbon dots for early warning of tumorigenesis, Adv. Mater. 33 (2021), 2005096, https://doi.org/10.1002/adma.202005096.
[44] Y. Dong, H. Pang, H. Bin Yang, C. Guo, J. Shao, Y. Chi, C.M. Li, T. Yu, Carbon-based dots co-doped with nitrogen and sulfur for high quantum yield and excitation-independent emission, Angew. Chem. Int. Ed. 52 (2013) 7800–7804, https://doi.org/10.1002/anie.201301114.
[45] H. Liu, Z. Li, Y. Sun, X. Geng, Y. Hu, H. Meng, J. Ge, L. Qu, Synthesis of luminescent carbon dots with ultrahigh quantum yield and inherent folate receptor-positive cancer cell targetability, Sci. Rep. 8 (2018) 1–8, https://doi.org/10.1038/s41598-018-19373-3.
[46] S.N. Baker, G.A. Baker, Luminescent carbon nanodots: emergent nanolights, Angew. Chem. Int. Ed. 49 (2010) 6726–6744, https://doi.org/10.1002/anie.200906623.
[47] C.M. Carbonaro, R. Corpino, M. Salis, F. Mocci, S.V. Thakkar, C. Olla, P.C. Ricci, On the emission properties of carbon dots: reviewing data and discussing models, C — J. Carbon Res. 5 (2019) 60, https://doi.org/10.3390/c5040060.
[48] S. Qu, X. Wang, Q. Lu, X. Liu, L. Wang, A biocompatible fluorescent ink based on water-soluble luminescent carbon nanodots, Angew. Chem. 124 (2012) 12381–12384, https://doi.org/10.1002/ange.201206791.
[49] H. Lin, J. Huang, L. Ding, Preparation of carbon dots with high-fluorescence quantum yield and their application in dopamine fluorescence probe and cellular imaging, J. Nanomater. 5037243 (2019), https://doi.org/10.1155/2019/5037243.
[50] N. Papaioannou, A. Marinovic, N. Yoshizawa, A.E. Goode, M. Fay, A. Khlobystov, M.M. Titirici, A. Sapelkin, Structure and solvents effects on the optical properties of sugar-derived carbon nanodots, Sci. Rep. 8 (2018) 6559, https://doi.org/10.1038/s41598-018-25012-8.
[51] B. Zheng, Y. Chen, P. Li, Z. Wang, B. Cao, F. Qi, J. Liu, Z. Qiu, W. Zhang, Ultrafast ammonia-driven, microwave-assisted synthesis of nitrogen-doped graphene quantum dots and their optical properties, Nanophotonics 6 (2017) 259–267, https://doi.org/10.1515/nanoph-2016-0102.
[52] H. Peng, J. Travas-Sejdic, Simple aqueous solution route to luminescent carbogenic dots from carbohydrates, Chem. Mater. 21 (2009) 5563–5565, https://doi.org/10.1021/cm901593y.
[53] A.B. Bourlinos, A. Stassinopoulos, D. Anglos, R. Zboril, M. Karakassides, E.P. Giannelis, Surface functionalized carbogenic quantum dots, Small 4 (2008) 455–458, https://doi.org/10.1002/smll.200700578.
[54] P. Mirtchev, E.J. Henderson, N. Soheilnia, C.M. Yip, G.A. Ozin, Solution phase synthesis of carbon quantum dots as sensitizers for nanocrystalline TiO 2 solar cells, J. Mater. Chem. 22 (2012) 1265–1269, https://doi.org/10.1039/c1jm14112k.
[55] C.M. Carbonaro, R. Corpino, M. Salis, F. Mocci, S.V. Thakkar, C. Olla, P.C. Ricci, On the emission properties of carbon Dots : reviewing data and discussing models, J. Carbon Res. 5 (2019) 1–15, https://doi.org/10.3390/c5040060.
[56] J. Wang, P. Zhang, C. Huang, G. Liu, K.C.F. Leung, Y.X.J. Wáng, High performance photoluminescent carbon dots for in vitro and in vivo bioimaging: effect of nitrogen doping ratios, Langmuir 31 (2015) 8063–8073, https://doi.org/10.1021/acs.langmuir.5b01875.
[57] F. Arcudi, L. Dordevic, M. Prato, Synthesis, separation, and characterization of small and highly fluorescent nitrogen-doped carbon nanodots, Angew. Chem. Int. Ed. 55 (2016) 2107–2112, https://doi.org/10.1002/anie.201510158.
[58] L. Tang, R. Ji, X. Li, K.S. Teng, S.P. Lau, Energy-level structure of nitrogen-doped graphene quantum dots, J. Mater. Chem. C. 1 (2013) 4908–4915, https://doi.org/10.1039/c3tc30877d.
[59] R. Atchudan, T.N.J.I. Edison, M.G. Sethuraman, Y.R. Lee, Efficient synthesis of highly fluorescent nitrogen-doped carbon dots for cell imaging using unripe fruit extract of Prunus mume, Appl. Surf. Sci. 384 (2016) 432–441, https://doi.org/10.1016/j.apsusc.2016.05.054.
[60] J. Zhang, Y. Yuan, M. Gao, Z. Han, C. Chu, Y. Li, P.C.M. van Zijl, M. Ying, J.W.M. Bulte, G. Liu, Carbon dots as a new class of diamagnetic chemical exchange saturation transfer (diaCEST) MRI contrast agents, Angew. Chem. Int. Ed. 58 (2019) 9871–9875, https://doi.org/10.1002/anie.201904722.
[61] L. Qian, A.R. Thiruppathi, R. Elmahdy, J. van der Zalm, A. Chen, Graphene-oxide-based electrochemical sensors for the sensitive detection of pharmaceutical drug naproxen, Sensors 20 (2020) 1252, https://doi.org/10.3390/s20051252.
[62] Z.Q. Xu, L.Y. Yang, X.Y. Fan, J.C. Jin, J. Mei, W. Peng, F.L. Jiang, Q. Xiao, Y. Liu, Low temperature synthesis of highly stable phosphate functionalized two color carbon nanodots and their application in cell imaging, Carbon N. Y. 66 (2014) 351–360, https://doi.org/10.1016/j.carbon.2013.09.010.
[63] J. Yu, C. Liu, K. Yuan, Z. Lu, Y. Cheng, L. Li, X. Zhang, P. Jin, F. Meng, H. Liu, Luminescence mechanism of carbon dots by tailoring functional groups for sensing Fe3+ ions, Nanomaterials 8 (2018) 233, https://doi.org/10.3390/nano8040233.
[64] Y. Choi, B. Kang, J. Lee, S. Kim, G.T. Kim, H. Kang, B.R. Lee, H. Kim, S.H. Shim, G. Lee, O.H. Kwon, B.S. Kim, Integrative approach toward uncovering the origin of photoluminescence in dual heteroatom-doped carbon nanodots, Chem. Mater. 28 (2016) 6840–6847, https://doi.org/10.1021/acs.chemmater.6b01710.
[65] H. Wang, P. Sun, S. Cong, J. Wu, L. Gao, Y. Wang, X. Dai, Q. Yi, G. Zou, Nitrogen-doped carbon dots for “green” quantum dot solar cells, Nanoscale Res. Lett. 11 (2016) 1–6, https://doi.org/10.1186/s11671-016-1231-1.
[66] M.J. Talite, H.Y. Huang, K. Bin Cai, K.C. Capinig Co, P.A. Cynthia Santoso, S.H. Chang, W.C. Chou, C.T. Yuan, Visible-transparent luminescent solar concentrators based on carbon nanodots in the siloxane matrix with ultrahigh quantum yields and optical transparency at high-loading contents, J. Phys. Chem. Lett. 11 (2020) 567–573, https://doi.org/10.1021/acs.jpclett.9b03539.
[67] D. Qu, M. Zheng, J. Li, Z. Xie, Z. Sun, Tailoring color emissions from N-doped graphene quantum dots for bioimaging applications, Light Sci. Appl. 4 (2015) e364, https://doi.org/10.1038/lsa.2015.137.
[68] I.A. Baragau, N.P. Power, D.J. Morgan, T. Heil, R.A. Lobo, C.S. Roberts, M.M. Titirici, S. Dunn, S. Kellici, Continuous hydrothermal flow synthesis of blue-luminescent, excitation-independent nitrogen-doped carbon quantum dots as nanosensors, J. Mater. Chem. A. 8 (2020) 3270–3279, https://doi.org/10.1039/c9ta11781d.
[69] L. Deng, X. Wang, Y. Kuang, C. Wang, L. Luo, F. Wang, X. Sun, Development of hydrophilicity gradient ultracentrifugation method for photoluminescence investigation of separated non-sedimental carbon dots, Nano Res 8 (2015) 2810–2821, https://doi.org/10.1007/s12274-015-0786-y.
[70] H. Ding, J.-S. Wei, H.-M. Xiong, Nitrogen and sulfur co-doped carbon dots with strong blue luminescence, Nanoscale 6 (2014) 13817–13823, https://doi.org/10.1039/c4nr04267k.
[71] N. Daems, X. Sheng, I.F.J. Vankelecom, P.P. Pescarmona, Metal-free doped carbon materials as electrocatalysts for the oxygen reduction reaction, J. Mater. Chem. A. 2 (2014) 4085–4110, https://doi.org/10.1039/c3ta14043a.
[72] H.L. Tran, W. Darmanto, R.A. Doong, Ultrasensitive detection of tetracycline using boron and nitrogen co-doped graphene quantum dots from natural carbon source as the paper-based nanosensing probe in difference matrices, Nanomaterials 10 (2020) 1883, https://doi.org/10.3390/nano10091883.
[73] X. Liu, J. Han, X. Hou, F. Altincicek, N. Oncel, D. Pierce, X. Wu, J.X. Zhao, One-pot synthesis of graphene quantum dots using humic acid and its application for copper (II) ion detection, J. Mater. Sci. 56 (2021) 4991–5005, https://doi.org/10.1007/s10853-020-05583-6.
[74] V. Kuzmenko, N. Wang, M. Haque, O. Naboka, M. Flygare, K. Svensson,

P. Gatenholm, J. Liu, P. Enoksson, Cellulose-derived carbon nanofibers/graphene composite electrodes for powerful compact supercapacitors, RSC Adv. 7 (2017) 45968–45977, https://doi.org/10.1039/c7ra07533b.
[75] T. Wang, C.J. Reckmeier, S. Lu, Y. Li, Y. Cheng, F. Liao, A.L. Rogach, M. Shao, Gamma ray shifted and enhanced photoluminescence of graphene quantum dots, J. Mater. Chem. C. 4 (2016) 10538–10544, https://doi.org/10.1039/c6tc03100e.
[76] J. Schneider, C.J. Reckmeier, Y. Xiong, M. Von Seckendorff, A.S. Susha, P. Kasak, A.L. Rogach, Molecular fluorescence in citric acid-based carbon dots, J. Phys. Chem. C 121 (2017) 2014–2022, https://doi.org/10.1021/acs.jpcc.6b12519.
[77] M. Fu, F. Ehrat, Y. Wang, K.Z. Milowska, C. Reckmeier, A.L. Rogach, J.K. Stolarczyk, A.S. Urban, J. Feldmann, Carbon dots: a unique fluorescent cocktail of polycyclic aromatic hydrocarbons, Nano Lett. 15 (2015) 6030–6035, https://doi.org/10.1021/acs.nanolett.5b02215.
[78] H. Ding, H.M. Xiong, Exploring the blue luminescence origin of nitrogen-doped carbon dots by controlling the water amount in synthesis, RSC Adv. 5 (2015) 66528–66533, https://doi.org/10.1039/c5ra11796h.
[79] M.J. Krysmann, A. Kelarakis, P. Dallas, E.P. Giannelis, formation mechanism of carbogenic nanoparticles with dual photoluminescence emission, J. Am. Chem. Soc. 134 (2012) 747–750, https://doi.org/10.1021/ja204661r.
[80] Z.Q. Liu, H. Cheng, N. Li, T.Y. Ma, Y.-Z. Su, ZnCo2O4 quantum dots anchored on nitrogen-doped carbon nanotubes as reversible oxygen reduction/evolution electrocatalysts, Adv. Mater. 28 (2016) 3777–3784, https://doi.org/10.1002/adma.201506197.
[81] H. Wang, T. Maiyalagan, X. Wang, Review on recent progress in nitrogen-doped graphene: synthesis, characterization, and its potential applications, ACS Catal. 2 (2012) 781–794, https://doi.org/10.1021/cs200652y.
[82] L. Roldán, S. Armenise, Y. Marco, E. García-Bordejé, Control of nitrogen insertion during the growth of nitrogen-containing carbon nanofibers on cordierite monolith walls, Phys. Chem. Chem. Phys. 14 (2012) 3568–3575, https://doi.org/10.1039/c2cp23609e.
[83] Y. Dong, J. Shao, C. Chen, H. Li, R. Wang, Y. Chi, X. Lin, G. Chen, Blue luminescent graphene quantum dots and graphene oxide prepared by tuning the carbonization degree of citric acid, Carbon N. Y. 50 (2012) 4738–4743, https://doi.org/10.1016/j.carbon.2012.06.002.
[84] S. Zhu, Q. Meng, L. Wang, J. Zhang, Y. Song, H. Jin, K. Zhang, H. Sun, H. Wang, B. Yang, Highly photoluminescent carbon dots for multicolor patterning, Sensors, and Bioimaging, Angew. Chemie. 125 (2013) 4045–4049, https://doi.org/10.1002/ange.201300519.
[85] Z. Wang, Y. Lu, H. Yuan, Z. Ren, C. Xu, J. Chen, Microplasma-assisted rapid synthesis of luminescent nitrogen-doped carbon dots and their application in pH sensing and uranium detection, Nanoscale 7 (2015) 20743–20748, https://doi.org/10.1039/c5nr05804j.
[86] M. Sudolská, M. Dubecký, S. Sarkar, C.J. Reckmeier, R. Zbořil, A.L. Rogach, M. Otyepka, Nature of absorption bands in oxygen-functionalized graphitic carbon dots, J. Phys. Chem. C 119 (2015) 13369–13373, https://doi.org/10.1021/acs.jpcc.5b04080.
[87] H. Ding, X.H. Li, X.B. Chen, J.S. Wei, X.B. Li, H.M. Xiong, Surface states of carbon dots and their influences on luminescence, J. Appl. Phys. 127 (2020) 231101, https://doi.org/10.1063/1.5143819.
[88] Y. Li, H. Shu, X. Niu, J. Wang, Electronic and optical properties of edge-functionalized graphene quantum dots and the underlying mechanism, J. Phys. Chem. C 119 (2015) 24950–24957, https://doi.org/10.1021/acs.jpcc.5b05935.
[89] A. Xu, G. Wang, Y. Li, H. Dong, S. Yang, P. He, G. Ding, Carbon-based quantum dots with solid-state photoluminescent: mechanism, implementation, and application, Small 16 (2020) 2004621, https://doi.org/10.1002/smll.202004621.
[90] C.M. Carbonaro, D. Chiriu, L. Stagi, M.F. Casula, S.V. Thakkar, L. Malfatti, K. Suzuki, P.C. Ricci, R. Corpino, Carbon dots in water and mesoporous matrix: chasing the origin of their photoluminescence, J. Phys. Chem. C 122 (2018) 25638–25650, https://doi.org/10.1021/acs.jpcc.8b08012.
[91] C. Liu, Y. Jin, R. Wang, T. Han, X. Liu, B. Wang, C. Huang, S. Zhu, J. Chen, Indole carbonized polymer dots boost full-color emission by regulating surface state, IScience 23 (2020) 101546, https://doi.org/10.1016/j.isci.2020.101546.
[92] H. Ding, X.-H. Li, X.-B. Chen, J.-S. Wei, X.-B. Li, H.-M. Xiong, Surface states of carbon dots and their influences on luminescence, J. Appl. Phys. 127 (2020) 231101, https://doi.org/10.1063/1.5143819.
[93] D. Timmerman, J. Valenta, K. Dohnalová, W.D.A.M. De Boer, T. Gregorkiewicz, Step-like enhancement of luminescence quantum yield of silicon nanocrystals, Nat. Nanotechnol. 6 (2011) 710–713, https://doi.org/10.1038/nnano.2011.167.
[94] D. Timmerman, I. Izeddin, P. Stallinga, I.N. Yassievich, T. Gregorkiewicz, Space-separated quantum cutting with silicon nanocrystals for photovoltaic applications, Nat. Photonics 2 (2008) 105–109, https://doi.org/10.1038/nphoton.2007.279.
[95] R. Mcweeny, Methods of Molecular Quantum Mechanics, second ed., Academic Press, London, 1989.